SF 298 MASTER COPY KEEP THIS COPY FOR REPRODUCTION PURPOSES

REPORT DOCUMENTATION PAGE

Form Approved
OMB NO. 0704-0188

1. AGENCY USE ONLY *(Leave blank)*	2. REPORT DATE	3. REPORT TYPE AND DATES COVERED
	January 17, 2001	FINAL - 01 Jul 96 - 30 Jun 00

4. TITLE AND SUBTITLE

Permanent Holographic Gratings for Wavelength Division Filtering

5. FUNDING NUMBERS

DAAH04-96-1-0322

6. AUTHOR(S)

Dr. James P. Wicksted - Principal Investigator
Dr. George S. Dixon - Co-Principal Investigator

7. PERFORMING ORGANIZATION NAMES(S) AND ADDRESS(ES)

Oklahoma State University

8. PERFORMING ORGANIZATION REPORT NUMBER

9. SPONSORING / MONITORING AGENCY NAME(S) AND ADDRESS(ES)

U.S. Army Research Office
P.O. Box 12211
Research Triangle Park, NC 27709-2211

10. SPONSORING / MONITORING AGENCY REPORT NUMBER

ARO 36195.6-RT-DPS

11. SUPPLEMENTARY NOTES

The views, opinions and/or findings contained in this report are those of the author(s) and should not be construed as an official Department of the Army position, policy or decision, unless so designated by other documentation.

12a. DISTRIBUTION / AVAILABILITY STATEMENT

Approved for public release; distribution unlimited.

12 b. DISTRIBUTION CODE

13. ABSTRACT *(Maximum 200 words)*

The final report summarizes the major research accomplishments of this program. High quality glass samples have been grown with varying amounts of Eu_2O_3 and Al_2O_3. Glass fibers have also been made. A successful model of the grating kinetics that treats grating formation as the result of optically stimulated diffusion of small modifier ions was developed. Four-wave mixing (FWM) results indicate that the grating efficiency increases with both compositions, in agreement with our kinetics model. The FWM results show that the grating diffraction efficiency decreases with decreasing temperatures for Eu concentrations ≤10 mol %. However, an increase in diffraction efficiency is observed for the *Eu* concentration of 15 mol %. The grating efficiency is insensitive to temperatures above room temperature although the grating build-up time increases with higher temperature. The Raman and NMR dependence suggests an increase in NBOs and in 6-fold coordinated *Al* with increasing *Eu*, while a decrease in NBOs with an increase in 4-fold coordinated *Al* results with increasing *Al*. Ionic conductivity and Brillouin scattering measurements have also been performed. The effect of write beam and probe beam wavelengths on the formation of refractive index gratings in these glasses has also been studied. In addition, we have demonstrated the writing and recovery of holographic images in these glasses.

14. SUBJECT TERMS

Holographic refractive index gratings, rare-earth doped glasses

15. NUMBER IF PAGES

23 plus Appendix

16. PRICE CODE

17. SECURITY CLASSIFICATION OR REPORT	18. SECURITY CLASSIFICATION OF THIS PAGE	19. SECURITY CLASSIFICATION OF ABSTRACT	20. LIMITATION OF ABSTRACT
UNCLASSIFIED	UNCLASSIFIED	UNCLASSIFIED	UL

PERMANENT HOLOGRAPHIC GRATINGS FOR WAVELENGTH DIVISION FILTERING

FINAL PROGRESS REPORT

Drs. James P. Wicksted and George S. Dixon

January 16, 2001

U.S. ARMY RESEARCH OFFICE

CONTRACT/GRANT NUMBER: DAAH04-96-1-0322

OKLAHOMA STATE UNIVERSITY

APPROVED FOR PUBLIC RELEASE;

DISTRIBUTION UNLIMITED.

TABLE OF CONTENTS

FOREWORD

A systematic investigation of the characteristics of composition and processing that underlie the nonlinear scattering in rare-earth activated silicate glasses was undertaken during this four-year program. Permanent holographic gratings in these glass systems suggest potential applications as high-Q frequency selective filters.

Key questions answered by this research include: (i) how close can two laser-induced holographic gratings be before cross-talk interference results; (ii) how tunable and stable are these laser-induced gratings for different compositions and temperature. The Advanced Research Projects Agency has a strong interest in wavelength division multiplexing. This proposal included the synthesis and characterization of laser induced gratings in rare earth doped glasses. In particular, the characteristics of grating formation, stability, and erasure in addition to the ionic transport properties and phonon physics of these media that are important to these optical characteristics. Four-wave mixing experiments were utilized to determine the Bragg scattering efficiency of these laser gratings that are correlated to the host glass composition and the phonon structure of the glass network. In addition to the four-wave mixing measurements, Raman and Brillouin scattering measurements, as well as ionic conductivity and NMR measurements, were conducted on many of the rare-earth doped glass samples.

LIST OF APPENDICES, ILLUSTRATIONS, AND TABLES

A. STATEMENT OF THE PROBLEM STUDIED

To determine the concentration and temperature dependence of laser-induced holographic gratings in rare-earth doped alkali silicate glasses. Concentration changes in these glasses with europium content are given in Table 1. A four-wave mixing experimental setup was used for this study.

Table 1 Sample information

	SiO_2 (%mol)	Na_2O (%mol)	MgO (%mol)	Al_2O_3 (%mol)	Eu_2O_3 (%mol)	ρ (g/cm^3)	n @514.5nm	α (cm^{-1})
Bragg05	70	15	12	3	0	2.72	1.528	0.324
Bragg07	69.65	14.925	11.94	2.985	0.5	2.47	1.533	0.372
Bragg08	69.30	14.85	11.88	2.97	1	2.52	1.536	0.451
Bragg09	68.25	14.625	11.70	2.925	2.5	2.56	1.541	0.563
Bragg10	66.50	14.25	11.40	2.85	5	2.78	1.545	0.807
OSU-Eu7.5	64.75	13.875	11.10	2.775	7.5	2.94	1.554	0.986
OSU-Eu10	63	13.50	10.80	2.7	10	3.12	1.568	1.19
OSU-Eu15	59.50	12.75	10.20	2.55	15	3.33	1.610	1.48
OSU-Eu2.5	68.25	14.625	11.70	2.925	2.5	2.61	1.534	0.983
OSU-Eu5	66.50	14.25	11.40	2.85	5	2.87	1.537	1.29
F-Quartz	100					2.21	1.462	0.04

In addition to this major issue, several important objectives were also addressed in this research:

(i) Developing optics and kinetics models to make comparisons between our experimental four-wave mixing results and theory.
(ii) Determining how close two laser-induced images can be before cross-talk interference results.
(iii) Showing that gratings can be written and probed using different laser wavelengths.
(iv) Relating measurements, such as Raman scattering, Brillouin scattering, ionic conductivity, and NMR, to our understanding of the laser induced gratings in these rare-earth doped glass samples.
(v) Attempting to write laser-induced gratings in fibers of the same concentrations as bulk glass samples.

B. SUMMARY OF THE MOST IMPORTANT RESULTS

VOLUME GRATING PRODUCED BY INTERSECTING GAUSSIAN BEAMS IN AN ABSORBING MEDIUM: A BRAGG DIFFRACTION MODEL

A theoretical model, assuming pure phase gratings, was developed concerning the diffraction of a Gaussian probe beam by a volume grating formed by two intersecting Gaussian pump beams in an absorbing medium. The dependence of the Bragg diffraction efficiency on material parameters (sample thickness, absorption, and nonlinear refractive index) was shown in this model. Such a model more accurately reflects our experimental configuration and provides us with needed information as to how Bragg diffraction efficiencies should vary with crossing angle and laser beam spot size. This model allows the determination of the nonlinear change in the index of refraction Δn arising from permanent gratings induced in our samples. This can then be compared with a theoretical Δn which is obtained from a kinetics model, as described below.

KINETICS MODEL OF PHOTOINDUCED REFRACTIVE INDEX GRATINGS IN RARE-EARTH-SENSITIZED GLASSES

This model relates the refractive index modulation to an underlying modulation in the composition of the glass, particularly in the distribution of small modifiers. For simplicity, only one species of modifier is assumed to be mobile. In this picture, it suffices to calculate the density $M(x,t)$ of mobile modifiers to obtain the strength of the grating. One dimensional diffusion and drift along the grating axis are considered. The mobile modifiers are distributed over a uniform density of sites. The calculation is carried out in three stages: 1) first, the modifiers are taken to be neutral; 2) secondly, a uniform density D of deep traps is introduced that permanently immobilizes initially mobile modifiers; 3) finally, the modifiers are allowed to be charged so that drift under the influence of the space-charge field or an applied field must be included. The nonlinear change in the index of refraction is related to the density of mobile modifiers.

DETERMINING SPACING BETWEEN ADJACENT LASER-INDUCED GRATINGS AND STABILITY OF GRATINGS AND STORING HOLOGRAMS

We were able to write many holograms in Eu-doped silicate glass. After the recording was done, the object beam was blocked and the other beam (reference beam) was allowed to impinge on the sample in order to read out the stored information. The 465.8 nm line of an argon laser was used in writing with read beams of different wavelength. The spot size of the beams was w = 0.1mm, the total power used was in the range of 10-50 mW, the crossing angle of 10°, and the exposure time in the range of 10-30 seconds. The low power of the write-beam and the short exposure time indicate that this type of sample is good for practical applications such as storage devises. The closest distance (measured from the center of the previous grating region) that a grating or a hologram can be written without affecting a previous one (cross talk) was found to be on the order of w (0.1mm). More details of this can be obtained in Appendix 1 (*Holographic image storage in Eu3+ -doped alkali-aluminosilicate glasses*). A dark lifetime of these gratings is more than twenty months (see Fig. 4 in Appendix 1).

LASER-INDUCED GRATINGS WRITTEN AND PROBED WITH DIFFERENT LASER WAVELENGTHS

Laser-induced holographic gratings were recorded using different laser wavelengths from an argon-ion laser. The results for the maximum and permanent induced change in the index of refraction (Δn) as a function of write-beam wavelength are shown in Figure 1. Figure 1 also

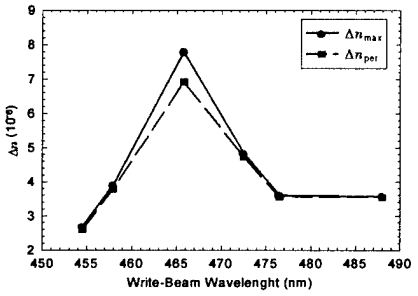

Fig. 1. Induced change in the index of refraction as a function of write-beam wavelength.

shows that the strongest grating was accomplished for λ_w=465.8 nm. This wavelength lies near the peak of the $7F_0$–$5D_2$ absorption transition. The surprising results were obtained for the off-resonance write-beam wavelengths.

Holographic images, written using the 465.8 nm line, could be read and probed using off-resonant wavelengths, as illustrated in Fig. 3 of Appendix 1 (*Holographic image storage in Eu3+ -doped alkali-aluminosilicate glasses*). Although the image quality is not as clear as when

reading the stored image using the same wavelength, nonetheless, quality images were still obtained indicating a longer reading lifetime when reading with off-resonant wavelengths.

CONCENTRATION DEPENDENCE OF LASER-INDUCED GRATINGS

Introduction

According to our (small-modifier diffusion) model[2] (see above model), sodium-ion-migration from the bright regions toward the dark regions is responsible for the formation of the permanent grating in these glasses. In sodium aluminosilicate glasses, it is known that ionic conductivity increases by increasing the *Al* concentration[3] (see Section on Ionic Conductivity Measurements). Therefore, we used glass samples with different *Al* and *Eu* concentrations and studied the strength of the grating as a function of the these concentrations. The samples have the following compositions: for *Al* variation $\mathbf{[0.15Na_2O - 0.12MgO - y\ Al_2O_3 - (0.73 - y)\ SiO_2]_{97.5} + [Eu_2O_3]_{2.5}}$, where y = 0.03, 0.06, 0.09, 0.15 and for *Eu* variation $\mathbf{[0.70SiO_2 + 0.15Na_2O + 0.12MgO + 0.03Al_2O_3]_{(100-x)} + [Eu_2O_3]_x}$, where x = 1.5, 2.5, 5.0, 7.5, 10.0, 15.0 mol.%. The samples have thicknesses between 2 to 4 mm.

Results and Discussion

The general procedure we used is as follows. The write-beams were kept on until the power of the diffracted signal reached its maximum. Then both write-beams were blocked over a 5-minute period to determine the transient component of the diffracted signal. This measurement was followed by unblocking one of the write-beams in order to start the erasing process. The power of the write-beam was the same during both the writing and the erasing processes. Most of the time, these steps were repeated twice during the same scan. When the writing process started, a diffracted signal appeared immediately followed by an increase in the signal intensity until it reached its maximum. The signal build-up usually occurred over a period of one to several minutes depending on the sample, the total power of the write-beams and the crossing angle. The diffracted signal was observed to decay slowly if the write-beams were kept on after the signal reached its maximum.

When Eu^{3+} is excited to the $^5D_2$ level, it decays to the lower ^5D_J (J=0,1) levels via nonradiative decay processes. The radiationless relaxation takes place through multiphonon emission of several high-energy phonons. The high-energy phonons provide the activation energy for some light modifiers to migrate in the glass network. The permanent grating is due to the permanent change in the index of refraction Δn, which, in turn, is a result of the migration of light modifiers like Na from the bright toward the dark regions. Here $\Delta n(x,t)_{per} \propto \Delta M(x,t)$, where M(x,t) is the density of the mobile modifiers as determined from our kinetics model[2].

Effects of Al_2O_3 Concentration

Fig. 2(a) shows that the change in the index of refraction increases as the Al_2O_3 concentration increases. The linear behavior of the Δn with Al_2O_3 indicates that *Al* is important in the formation of efficient grating. This will be seen clearly as we discuss these results later.

Fig. 2(b) displays the density of the mobile modifiers as a function of Al_2O_3 concentration. This result was obtained using the kinetics model[2] and the experimental data. To understand these results, we first should discuss how the Al_2O_3 enters the glass network. There is a general agreement that when the ratio of Al/Na is less than 1, the Al^{3+} substitutes for Si^{4+} in the glass network. This results in the

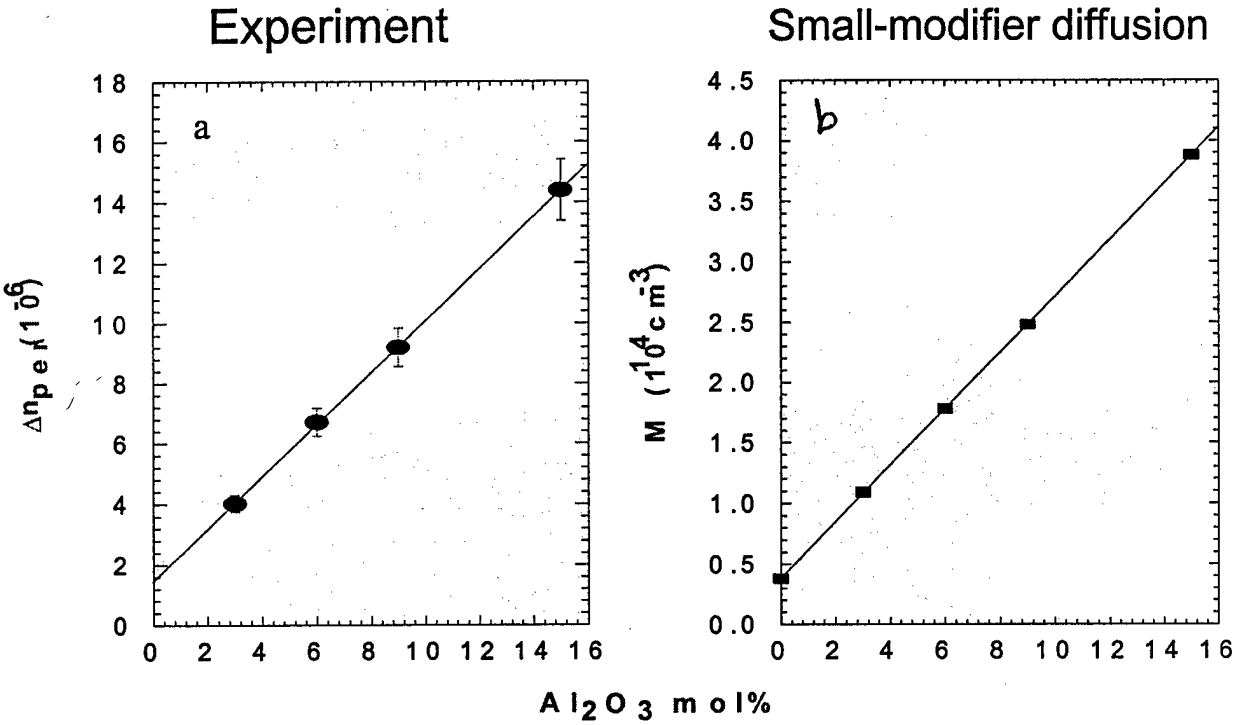

Fig. 2 The change in the index of refraction and the modifiers density as function of Al_2O_3 concentration.

elimination of one non-bridging oxygen. The Na^+ ion then associates itself with the Al^{3+} ion. A diagram showing the AlO_4 tetrahedral group is displayed in Fig. 3. The activation energy of Na^+ associated with Al^{3+} is smaller than that of Na^+ associated with a non-bridging oxygen. This is due mainly to the localization of the charge on the AlO_4 group. The increase in the Δn with the increase of *Al* concentration can be explained as follows. According to our model, the increase in Δn is a measure of the number of modifiers that have been moved from the bright toward the dark regions. When the *Al* concentration increases, the activation energy for the Na^+ decreases[3,4], and as a result, more Na^+ migrate from the bright region toward the dark regions. The linear increase is due to the fact that every AlO_4 group attracts one Na^+. This also shows that the Na^+ ions associated with the AlO_4 group are the main constituents that participate in the migration process. Note that the decrease in activation energy with the increase in Al_2O_3 concentrations is also consistent with the ionic conductivity measurements which is presented later in this report.

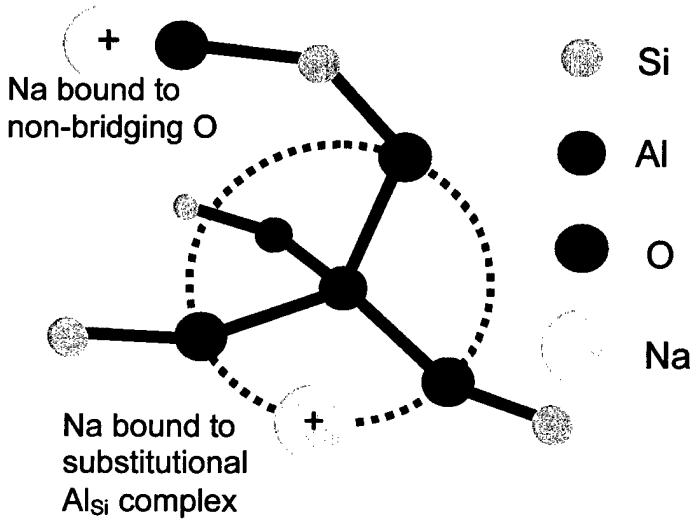

Fig. 3. A schematic diagram shows AlO_4 tetrahedral group.

Effects of Eu_2O_3 Concentration

As the Eu_2O_3 concentration increased, a substantial increase in the grating strength was observed. Fig. 4(a) shows how the permanent change in the index of refraction, Δn_{per}, behaved as the Eu content increased. Notice that Δn_{per} increased nonlinearly for Eu_2O_3 concentration

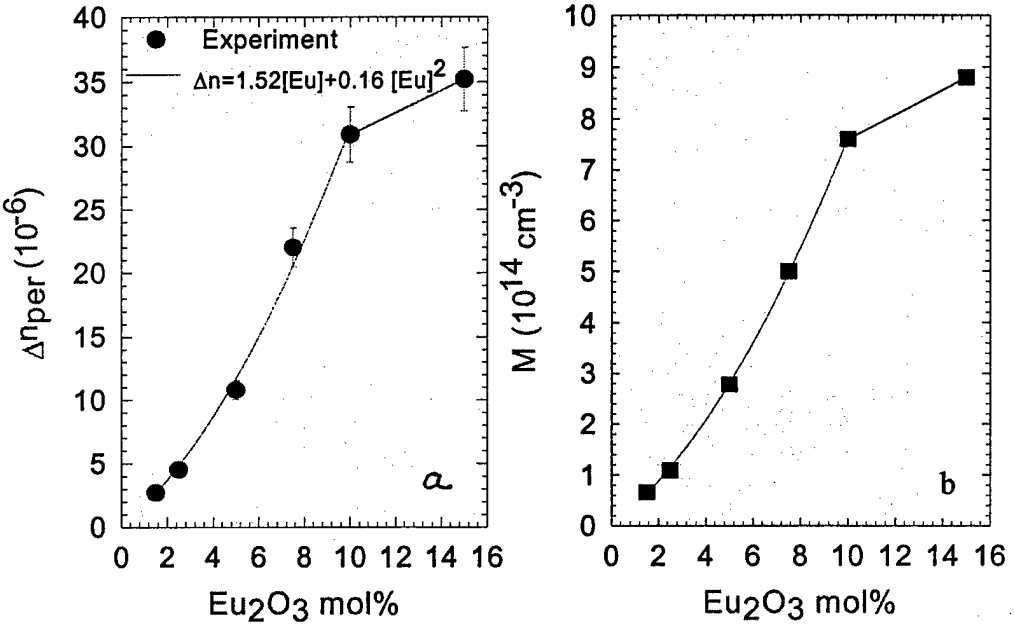

Fig. 4 The permanent change in the index of refraction (a) and the corresponding density of the mobile modifiers (b) as function of the Eu_2O_3 concentration.

between 2.5 and 10 mol.%, after which it starts to saturate. Figure 4(b) shows the density of the mobile modifiers, M, as a function of Eu_2O_3 concentration. Its behavior is similar to that of Δn_{per}. This is to be expected because Δn_{per} is directly proportional to M. The increase in the Δn_{per} with the increase of *Eu* concentration can be explained as follows. According to our model, the increase in Δn is a measure of the number of modifiers that have been moved from the bright toward the dark regions. When the *Eu* concentration increases, the *Eu* occupies sites close to those of *Na*, and as a result, the number of *Na* that will be able to move will increase. Also, with the increase in the *Eu* concentration, the energy provided to the system increases. Therefore, *Na* farther from *Eu* sites or in deeper traps will obtain the energy needed for the migration process. This accounts for the small quadratic behavior of Δn_{per}.

The transient component of the grating is attributed to a population grating[5]. The increase in the Δn_{tran} with the increase of *Eu* concentration is due to the increase in the excited Eu^{3+}. The fluorescence data showed that the local environment of Eu^{3+} changes with the *Eu* concentration. This is due mainly to the change in the crystal field at the site of Eu^{3+}. The signal build-up rate is

proportional to the number of the hot-phonons because the latter is the source of energy for the migration process. Therefore, the larger the energy in the system, the more rapid the migration process will be. Also, the larger the changes in the transient index of refraction, the larger the number of the hot phonons. This is due to the fact that the excited Eu^{3+} decays nonradiatively from the $^5D_2$ to the $^5D_0$, intermediate state, producing several high-energy phonons. Previously, it has been established[5] that the excited Eu^{3+} to the $^5D_0$ is responsible for the transient grating. This shows the basis for the linear relation between the build-up rate and the transient change in the index of refraction.

TEMPERATURE DEPENDENCE OF LASER-INDUCED GRATINGS

The experimental setup is the same as previously described. Here, the crossing angle (measured in air) is 3.87°, respectively. The CW argon laser operating in the TEM_{00} mode radiated the 465.8 nm line, which excited the Eu^{3+} ions to the $^5D_2$ level. The temperature at which we performed measurements is in the range from room temperature to liquid nitrogen temperature.

Figs. 5 and 6 show how the initial maximum P_{max} changed as we lowered the temperature of the samples with different Eu^{3+} concentrations in different ranges of temperature. The range of temperature is from room temperature to -33 °C for Fig. 5 and from room temperature to -183 °C for Fig. 6, respectively. There are two trends for the different samples. For the Eu15 sample, the initial maximum increased as the temperature was lowered. For the other samples, Eu5, Eu7.5

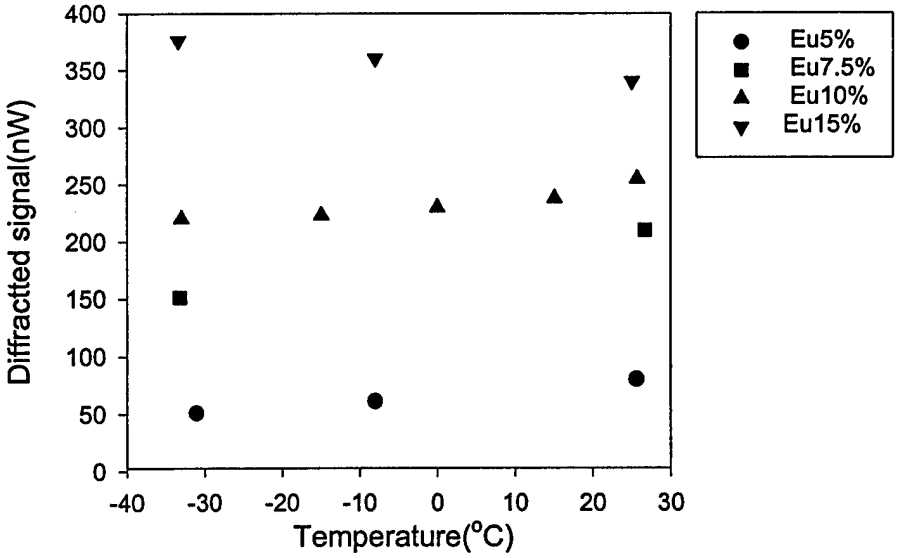

Fig. 5. The temperature dependence of P_{max}, $2\theta_w$=8.75°, P_w=50mW.

and Eu10, the initial maximum decreased at the lowered temperature.

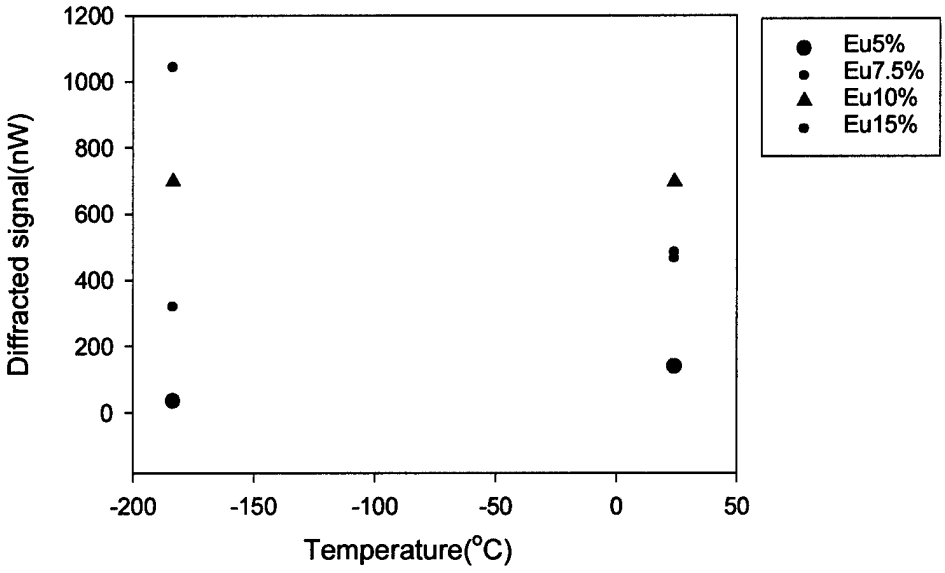

Fig. 6. The temperature dependence of P_{max}, $2\theta_{\omega}$=3.87°C.

Measurements have also been performed for temperatures above room temperature to about 92°C. The experimental setup is the same except that the crossing angle is changed to 5.145°. It should be noted that, unlike temperatures below room temperature, there is no significant change in the diffracted grating efficiency above room temperature for glass samples with varying Eu^{3+} concentrations. However, changes are seen in the build-up time of the grating formation and the rewriting of a laser grating following erasure.

Fig. 7 presents the results of the build-up time for the samples with Eu^{3+} concentrations of 5, 7.5, 10 and 15 mol % at different temperatures of grating formation. The build-up time is defined as how long it takes the diffracted signal to reach the maximum. As indicated by the figure, when the grating formation temperature increases, the build-up time increases also. It can be explained by the increase of acoustic phonons when the temperature increases.

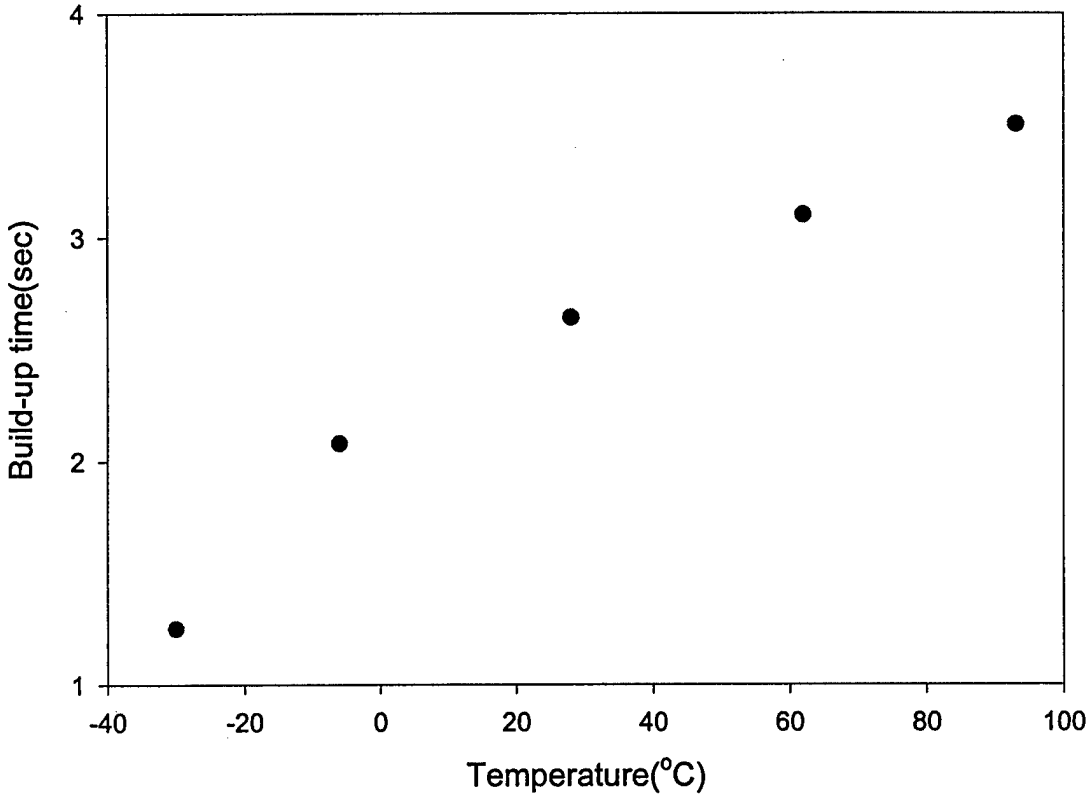

Fig. 7. Temperature dependence of build-up time of the maximum grating at different temperatures, Eu 15%, $2\theta_w$=5.145°.

In the rewrite procedures of a laser-induced grating, the sample is allowed to reach its maximum diffracted efficiency, after which a single write beam erases this initial grating.. After the grating has been erased for two minutes by one write beam, the second write beam is turned on allowing the grating to be generated again. During this rewrite process, we find much stronger gratings are achieved at higher temperatures. This behavior is seen for samples with varying Eu^{3+} concentrations of 5, 7.5, 10, and 15 mol %.

OTHER MEASUREMENTS

Raman Scattering

Raman scattering measurements were conducted on glass samples with variations in Eu_2O_3 and Al_2O_3 (see Table 1 and formulas in the introduction section on of the laser-induced grating measurements).

The **effect of increasing the Eu_2O_3 composition** shows an increase in the number of non-bridging oxygen bonds. The shift of 840–1200 cm^{-1} Raman band to lower wave-numbers with increasing rare earth oxide content indicates that the average number of NBO / tetrahedron increases with increasing rare earth oxide concentration.[6] Recent results indicate that the increase is due to a compensation of the non-bridging oxygen (NBO) via the Eu^{3+} ion with a corresponding decrease of NBOs compensated by Na or Mg. It is also seen that structures with two NBOs also increase in the glass network. In addition, the appearance of new low-frequency modes takes place suggesting that Eu^{3+} ions may occupy different sites and form high-order coordination spheres.[7] Finally, there is an indication of an increase in Raman modes affiliated with six-fold coordinated Al, $(AlO_6)^{3-}$, in the mid-frequency Raman structure.

The **effect of increasing the Al_2O_3 composition** shows a decrease in the NBO structures. This is an indication of a more connective system, where the $(AlO_4)^-$ tetrahedral group previously described becomes a former in the glass network. This provides a need for an alkali ion compensator, such as Na^+, which, because of the weaker bonding with $(AlO_4)^-$ as compared to a NBO, more efficient glass laser-induced gratings result.

NMR

With an increase of Eu_2O_3, content, the number of Eu–O–Si and Eu–O–Al bonds increases. There is also growth in the number of 6-fold coordinated aluminum complexes, while the number of 4-fold coordinated aluminum complexes decreases so that the net effect is overall enhancement of the number of NBOs since 6-fold coordinated Al is a network modifier.[8,9] This is consistent with the Raman scattering results.

With an increase of AL_2O_3 content, an increase in the 4-fold coordinated aluminum results with a corresponding decrease in 6-fold aluminum. Once again, this is completely consistent with the Raman scattering results, where a decrease in NBO's is seen since $(AlO_4)^-$ is a network former.

Ionic Conductivity

In general, the change in ionic conductivity with composition of the glass system can result from two physical characteristics; first, the binding energy of the alkali ion changes, second, the strain energy of the network changes. The latter is attributed to the fact that conduction channels in the glass can either be widened or narrowed, or changed in their number as the composition is altered.

The effect of increasing the Eu_2O_3 content shows an increase of the activation energy that indicates a decrease in the conductivity of the glass. There are several reasons that might explain this behavior. One obvious reason is that an increase in Eu_3O_2 inherently decreases the Na_2O concentration, thus decreasing the availability of mobile ions. As for the glass structure, the bonding is stronger between Eu^{3+}-NBO compared to the bonding of Na^+-NBO; therefore, Eu^{3+} ions are immobile and do not contribute to the conductivity. This also results in Eu^{3+} occupation of NBO interstices close to those of Na^+ ions. The immobile Eu ions then block the movement

of Na^+ ions. Last, the inter-atomic distance between the Si-O bonding is comparable to the atomic radius of the Eu^{3+}. During glass formation, it is possible for Eu^{3+} to get intertwined within the glass structure so that it does not locally charge compensate any of the NBOs. The NBOs, which are not charge compensated, act as holes that trap mobile modifiers, thus increasing the average activation or binding energy. In contrast, four-wave mixing experiments involve a different process in ion hopping as compared to ionic conductivity studies. In ionic conductivity, the temperature dependent oscillation of the mobile ions along with the electric field is the primary mechanism of ion hopping. Likewise, the europium is the primary thermal source in four-wave mixing studies; therefore, the opposite results between four-wave mixing experiments and ionic conductivity experiments are expected. Furthermore, it has also been shown that Mg ions in four-wave mixing do contribute to the ion migration. In ionic conductivity studies, the Mg ions impede the mobility of Na ions.

The effect of increasing the Al_2O_3 content increases the ionic conductivity within the glass. In most studies of sodium aluminosilicate glass, a slight decrease in conductivity is observed with the initial substitution of aluminum for silicon up until (Al/Na) ≈ 0.2 , after which the conductivity increases with the substitution until (Al/Na) ≈ 1. Since this increase causes an increase in $(AlO_4)^-$ complexes and a decrease in the number of NBO's, the Na^+ ions become more weakly bound to the former, indicating a lower activation energy. This is consistent with the Raman scattering and NMR measurements.

The effect of increasing the Na_2O content at the expense of SiO_2 is given by the following composition formula: (in mole percent) $\mathbf{[X\ Na_2O - 0.12\ MgO - 0.03\ Al_2O_3 - (0.85 - X)SiO_2]_{97.5} + [\ Eu_2O_3]_{2.5}}$ where **X = 0, 15, 20, 25**. The trend of the activation energy is downward, indicating an increase in the ionic conductivity as the Na concentration increases. As the Na concentration increases, one expects the sites of lowest energy to fill first; thus, higher Na concentration samples have lower average activation energies due to the greater fraction of Na in shallow sites.

Brillouin Scattering

Brillouin scattering measurements have only been performed on the series of glass structures with varying Eu_2O_3. It is seen that as the Eu^{3+} concentration increases, both the transverse (C_{44}) and longitudinal (C_{11}) acoustic elastic constants in the glass structure increase. These results are given in Table 2.

Table 2 Brillouin scattering results for glasses with increasing Eu^{3+} concentration

Eu^{+3} %	C_{11} (TPa)	C_{44} (TPa)	B (TPa)	Y (TPa)	$\underline{\sigma}$
Brg05	0.840	0.300	0.440	0.734	0.222
Brg07	0.745	0.259	0.399	0.640	0.233
Brg08	0.773	0.268	0.415	0.662	0.234
Brg09	0.799	0.277	0.431	0.683	0.236
Brg10	0.872	0.304	0.467	0.749	0.233
F-quartz	0.775	0.302	0.372	0.713	0.171

The elastic coefficients, C_{11} and C_{44}, were determined from the values of longitudinal and transverse acoustic sound velocities. These results are given in Table 2. Since C_{11} and C_{44} represent compressibility and shear constants, respectively, this result indicates that the glass becomes harder when the Eu^{3+} concentration is increased.

Some other important material properties such as Young's modulus (E), corresponding to the elasticity of the material, Poisson's ratio (σ), representing the atomic structure information, and adiabatic bulk modulus (B), corresponding to the material compressibility, can be derived from the elastic coefficients (See Table 2). Both the Young's and bulk moduli increase indicating that the glasses become more incompressible with increasing Eu^{3+} concentration. The larger value of Poisson's ratio, compared with fused quartz as shown in Table 2, implies that the overall bonding in the glass becomes more ionic. This is in agreement with both the Raman and NMR results since an increase in NBO structure plus the coordination change in the glass network from a glass former, $(AlO_4)^-$, to a modifier, $(AlO_6)^{3-}$, is indicative of a system becoming more ionic.

LASER-INDUCED GRATINGS IN FIBERS

Attempts have been made to write laser-induced gratings in fibers having the same concentrations as the bulk samples previously studied. The glass material that remained after core drilling the bulk glass material in the platinum crucible was heated to 1650 °C. At this temperature the bottom-loading furnace was raised and a platinum wire was lowered into the crucible after which the wire was pulled at a constant rate to obtain the fiber. This way, we were able to draw fibers with 1-2 meter length. The optical properties of the fiber looked reasonably good, even though the fibers were not cladded. Laser gratings were attempted using the same interferometric technique used in the bulk glass samples. The fibers were then placed within an absorption spectrophotometer to determine if any transmission changes occurred in near infrared wavelengths do to the creation of gratings within the fiber core. However, no changes have been observed up to this point. It is assumed that the volume occupied by the grating is not large enough to result in suitable Bragg reflection at the infrared wavelengths.

Further attempts at forming these gratings will be undertaken. First, the fiber will be placed in an index matching solution in order to reduce reflections losses at its outer region when write beams are incident using the interferometric configuration. Second, the fiber will be transported while being subjected to the two write beams in order to make laser gratings of larger volume.

C. LIST OF ALL PUBLICATIONS

Volume Grating by Intersecting Gaussian Beams in an Absorbing Medium: A Bragg Diffraction Model, by Abdulatif Y. Hamad and James P. Wicksted. Published in Optics Communications, Vol. 138, pages 354-364, 1997.

Laser-induced transient and permanent gratings in Eu^{3+} -doped dual alkaline earth silicate glasses, by Abdulatif Y. Hamad, James P. Wicksted, George S. Dixon, and L. P. de Rochemont. Published in the Journal of Non-Crystalline Solids **241**, 59-70 (1998).

Kinetics of holographic refractive-index gratings in rare-earth-sensitized glasses, by George S. Dixon, Abdulatif Y. Hamad, and J. P. Wicksted. Published in Physical Review B **58**, 200-205 (1998).

The effect of write-beam wavelength on the grating formation in Eu^{3+}-doped alkali-silicate glasses, by Abdulatif Y. Hamad, James P. Wicksted, and George S. Dixon. Published in Optical Materials **12**, 41-45 (1999).

Holographic image storage in Eu^{3+}-doped alkali-aluminosilicate glasses, by Abdulatif Y. Hamad and James P. Wicksted. To be published in Applied Optics.

Structural Characterization of Eu_2O_3-MgO-Na_2O-Al_2O_3-SiO_2 Glasses with Varying Eu_2O_3 Content: Raman and MAS NMR Studies, by Zhandos N. Utegulov, Margaret A. Eastman, Abdulatif Y. Hamad, James P. Wicksted, and George S. Dixon. Submitted to the Journal of Non-Crystalline Solids.

Z. N. Utegulov, M. A. Eastman, G. Shen, A. Y. Hamad, J. P. Wicksted, and G. S. Dixon, "Raman, NMR and Brillouin Studies of Eu^{3+}-Doped Soda Magnesium Aluminosilicate Glasses." Presented at the Glass & Optical Materials Division Fall Meeting, Corning, New York, October 1-4, 2000.

X. W. Zhang, A.Y. Hamad, G.S. Dixon, and J.P. Wicksted, "Temperature Dependence of Laser Induced Gratings in Eu-Doped Glasses." Presented at the 2000 Annual Meeting, Optical Society of America, Providence, Rhode Island, October 22-26, 2000.

A.Y. Hamad, J.P. Wicksted, G.S. Dixon, C.A. Hunt, and J.J. Martin, "The influence of Al_2O_3 concentration on the grating kinetics in Eu^{3+}-doped alkali-silicate glass." Presented at the 1998 Annual Meeting, Optical Society of America, Baltimore, Maryland, October 4-9, 1998.

A.Y. Hamad, J.P. Wicksted, G.S. Dixon, C.A. Hunt, and J.J. Martin, "The effect of Eu^{3+} concentration on the grating efficiency in alkali-silicate glass." Presented at the 1998 Annual Meeting, Optical Society of America, Baltimore, Maryland, October 4-9, 1998.

D. LIST OF ALL PARTICIPATING SCIENTIFIC PERSONNEL SHOWING ANY ADVANCED DEGREES EARNED BY THEM WHILE EMPLOYED ON THE PROJECT

Dr. James P. Wicksted, Principal Investigator

Dr. George S. Dixon, Co-Principal Investigator

Mr. Abdulatif Y. Hamad, graduate student, July 1, 1996 - July 31, 1996
Ph.D. awarded July 1996, Honorable Mention for the Summer 1996 Research Excellence Award

Mr. Shabbir M. Mian, graduate student, May 15, 1996 - August 15, 1996
Ph.D. awarded December 1996

Ms. Lynett Rock, graduate student, May 15, 1996 - July 31, 1996.
MS awarded July, 1996

Dr. Abdulatif Y. Hamad, Post doctoral fellow, August 1, 1996 - December 31, 1999; Assistant Visiting Professor, August 15, 2000 - December 31, 2000

Dr. Steven Paulin, Post doctoral fellow, August 1, 1996 - December 31, 1996

Mr. Zhandos Utegulov, graduate student, MS candidate, May 15, 1997 - May 31, 1999 **(Received MS in May 1999)**; graduate student, Ph.D. candidate, June 1 - December 31, 1999

Mr. Jason Paxton, graduate student, Ph.D. candidate, May 15, 1998 - December 31, 1999 **(Received MS in December 1999)**

Mr. Michael Hogsed, graduate student, MS candidate, May 15, 1998 - May 31, 1999 **(Received MS in May 1999)**

Mr. Abdur Rahman, graduate student, MS candidate, January 1, 1999 - July 30, 2000 **(Received MS in July 2000)**

Mr. Robert Ascio, graduate student, MS candidate, May, 1999 - December 2000 **(Received MS in December 2000)**

Mr. Xiwang Zhang, graduate student, MS candidate, May 15, 1999 - December 2000

Ms. Rumana Yaqub, graduate student, Ph.D. candidate, May 15, 2000 - December 31, 2000

REPORT OF INVENTIONS

NONE

BIBLIOGRAPHY

[1]A.Y. Hamad and J. P. Wicksted, Opt. Commun. **138**, 354 (1997).
[2]G. S. Dixon, A. Y. Hamad, and J. P. Wicksted, Phys Rev. B **58**, 200 (1998).
[3]C. H. Hsieh and H. Jain, J. Non-Cryst. Solids **183**, 1 (1995)
[4]G. N. Greaves and K. L. Ngai, Phys. Rev. B **52**, 6358 (1995)
[5]A. Y. Hamad, J. P. Wicksted, and G. S. Dixon, J. Non-Cryst. Solids **241**, 59 (1998).
[6] J.T.Kohli *et al.,* Phys. and Chem.of Glasses **34**, (1993).
[7] Tanabe *et al.*, J. Am. Ceram. Soc. **73**, 1733 (1990).
[8] S. Brawer and W. White, J. of Non - Cryst. Solids **23**, 261 (1977).
[9] D. C. Mckeown et al., J. of Non-Cryst. Solids **68**, 361 (1984).

APPENDIX 1

Holographic image storage in Eu^{3+} -doped alkali-aluminosilicate glasses